Solid State Ionics 293 (2016) 18–26

Contents lists available at ScienceDirect

Solid State Ionics

journal homepage: www.elsevier.com/locate/ssi

New promising NASICON material as solid electrolyte for sodium-ion batteries: Correlation between composition, crystal structure and ionic conductivity of $Na_{3+x}Sc_2Si_xP_{3-x}O_{12}$

M. Guin [a,*], F. Tietz [a,b], O. Guillon [a,b,c]

[a] Forschungszentrum Jülich GmbH, Institute of Energy and Climate Research (IEK-1): Materials Synthesis and Processing, D-52425 Jülich, Germany
[b] Helmholtz-Institute Münster, c/o Forschungszentrum Jülich GmbH, D-52425 Jülich, Germany
[c] Jülich Aachen Research Alliance, JARA-Energy, Germany

ARTICLE INFO

Article history:
Received 11 March 2016
Received in revised form 2 June 2016
Accepted 7 June 2016
Available online 15 June 2016

Keywords:
Ionic conductivity
NASICON
Sodium
Scandium
Solid electrolyte
Battery

ABSTRACT

In the search for novel sodium-ion conductors to be used in batteries for grid application, the thoroughly studied class of NASICON materials is of great interest due to compositional diversity and high ionic conductivity. The solid solution $Na_{3+x}Sc_2(SiO_4)_x(PO_4)_{3-x}$ with $0.05 \le x \le 0.8$ was investigated for the first time. The various compositions were synthesized by solid state reaction and their crystallographic and electrical properties were measured. As a result, one of the best sodium-conductive NASICON materials to date was obtained for $x = 0.4$ ($\sigma_{Na,Total} = 6.9 \times 10^{-4}$ S cm^{-1} at 25 °C). Furthermore, the importance of the sodium concentration and size of lattice parameters on the ionic conductivity were investigated. The bulk ionic conductivity was correlated with the structural parameters along the conduction pathway of the sodium ions and confirm the key influence of the interatomic Na–O distances on sodium ion transport.

1. Introduction

In 1976, Hong et al. introduced the term NASICON [1,2] to describe the very high ionic conductivity in $Na_3Zr_2Si_2PO_{12}$. This term is now used for all ceramic materials with the same crystal structure and the general composition $A_{1+2x+y+z}M^{(II)}_xM^{(III)}_yM^{(IV)}_{2-x-y}Si_zP_{3-z}O_{12}$ where A is usually a mono- or divalent cation (here, A = Na) and M are divalent, trivalent or tetravalent cations; P can also be substituted with Si or As. The materials belonging to the NASICON family are very attractive because of their compositional diversity leading to many possible applications, such as electrode materials or solid electrolytes in batteries as tested in an all-NASICON battery by Lalère et al. [3], Cl_2 and CO_2 sensors [4,5], or photoluminescent devices [6]. The conductivity of the NASICON materials is strongly related to their Na concentration and their crystallographic structure, which is influenced by the size of the M cations. It has been concluded from a literature survey [7] that the average ionic radius of M cations should be close to the ionic radius of Zr, i.e. $r_{Zr} = 0.72$ Å [8], in order to obtain highly conductive materials comparable to β- and β″-alumina [9,10]. In addition, the NASICON materials with the highest sodium ion conductivity contain 3–3.5 mol Na per formula unit and show a monoclinic distortion of the crystallographic lattice [7].

Following these guidelines for designing sodium ion conductors, the new solid solution $Na_{3+x}Sc_2Si_xP_{3-x}O_{12}$ (abbreviated hereafter as $NSSiP_x$) was investigated. The ionic radius of Sc of 0.745 Å [8] is close to the ionic radius of Zr and the presence of the trivalent Sc leads to a high amount of Na per formula unit. The introduction of Si in the highly conductive $Na_3Sc_2(PO_4)_3$ (2.3×10^{-5} S cm^{-1} at room temperature) [11] was inspired by the work of Hong on $Na_{1+x}Zr_2Si_xP_{3-x}O_{12}$ [1] and of Vogel et al. on $Na_{1+x}Hf_2Si_xP_{3-x}O_{12}$ [12]. In both cases, the substitution with Si in the structure led to a significant increase in conductivity. Different structural parameters were correlated with the measured ionic conductivity in order to better understand the impact of Si substitution on the Na^+ transport in the scandium-based NASICON materials.

2. Experimental

All compositions were synthesized via conventional solid state reaction. A stoichiometric homogenized mixture of $NH_4H_2PO_4$ (Merck KGaA, 99%), Sc_2O_3 (Projector GmbH, 99.5%), Na_2CO_3 (Alfa Aesar GmbH & Co KG, 99.5%), and SiO_2 (Alfa Aesar GmbH & Co KG, 99.8%) was heated with 300 K h^{-1} to 900 °C for 4 h. After grinding, the powder was again annealed for 20 h between 1280 °C and 1350 °C depending on the composition [11,13–15]. The obtained powder was milled and pressed into pellets (13 mm in diameter, approximately 2–5 mm height) and sintered at the annealing temperature of the powder for 10 h.

* Corresponding author.
E-mail address: m.guin@fz-juelich.de (M. Guin).

http://dx.doi.org/10.1016/j.ssi.2016.06.005
0167-2738/

The purity of the samples was controlled by X-ray diffraction (XRD) measurements (Bruker D4 ENDEAVOR diffractometer, Cu K_α radiation). The powder patterns were analyzed by Rietveld refinements using the Jana program [16] to determine lattice parameters, atomic positions and site occupancies.

The stoichiometry of the materials was controlled by inductively coupled plasma optical emission spectroscopy (ICP-OES) using the Thermo Scientific iCAP7600 spectrometer with optical scale and CID semi-conductor detector, axial und radial reflection, and wavelengths between 166 nm and 847 nm. 10 g of powder were mixed to 0.25 g lithium borate in a platinum crucible and heated for 0.5 h at 1000 °C. The liquefied material was dissolved in 30 mL HCl (5%) and filled to 50 mL volume.

Gold electrodes were sputtered on the surfaces of the pellets for conductivity measurements and the samples were put into Swagelok cells in an Ar-filled glovebox. The ionic conductivity from −30 to 30 °C was determined from impedance spectroscopy data measured with a multi-potentiostat VMP-300 from Bio-Logic SAS, France. The frequency range used was 1 Hz–7 MHz at intervals of 20 points per decade with an amplitude of 100 mV. The ionic conductivity from 30 to 400 °C was measured in argon (ProGasMix from NorECs) with the Alpha-A high performance modular measurement system (Novocontrol Technologies).

3. Results and discussion

3.1. Crystal structure

$NSSiP_x$ was synthesized in the compositional range of $0.05 \le x \le 0.8$. For $x \ge 0.1$, $NSSiP_x$ crystallizes with rhombohedral structure at room temperature (Fig. 1a). $NSSiP_{0.05}$ is a mixture of rhombohedral and monoclinic phases as shown in Fig. 1b, in which the XRD patterns of the samples $NSSiP_{0.05}$ and $NSSiP_{0.1}$ are enlarged for the diffraction angles between 18° and 30°. The appearance of three reflections at $2\theta = 19.5°$ and two reflections at $2\theta = 28°$ are characteristic for the presence of the monoclinic phase in the powder [17].

The stoichiometry of the $NSSiP_x$ compounds determined by ICP-OES is summarized in Table 1. The semi-quantitative results were normalized to 2 mol Sc/formula unit.

Table 1
Composition of the $NSSiP_x$ compounds determined by ICP-OES (experimental errors in the last digits are given in brackets).

Compound	Composition determined by ICP-OES
$NSSiP_{0.1}$	$Na_{2.90(2)}Sc_2Si_{0.109(8)}P_{2.90(2)}O_{11.9}$
$NSSiP_{0.2}$	$Na_{2.99(5)}Sc_2Si_{0.219(6)}P_{2.90(7)}O_{12.2}$
$NSSiP_{0.3}$	$Na_{3.02(7)}Sc_2Si_{0.291(8)}P_{2.71(8)}O_{11.9}$
$NSSiP_{0.4}$	$Na_{3.12(6)}Sc_2Si_{0.388(9)}P_{2.58(5)}O_{11.8}$
$NSSiP_{0.5}$	$Na_{3.34(8)}Sc_2Si_{0.49(1)}P_{2.46(5)}O_{11.8}$
$NSSiP_{0.6}$	$Na_{3.40(8)}Sc_2Si_{0.60(1)}P_{2.43(5)}O_{12.0}$
$NSSiP_{0.8}$	$Na_{3.51(8)}Sc_2Si_{0.80(2)}P_{2.16(5)}O_{11.8}$

It is noticeable that the amount of Na per formula unit was lower than expected for all the compounds. This is due to small weight losses during synthesis caused by the evaporation of sodium at temperatures above 1200 °C. The amount of oxygen per formula unit was not determined experimentally but calculated to compensate the charges.

The Rietveld refinements of all the compositions from Table 1 were carried out for $10° \le 2\theta \le 140°$ with full-matrix least-square against F^2 [18]. The starting parameters of the crystal structure were taken from the rhombohedral high-temperature structure of $Na_3Sc_2(PO_4)_3$ described by Boilot et al. [17] and the Pseudo-Voigt profile function was used. All atomic positions, lattice parameters and thermal displacement parameters could be refined for Sc, P/Si and O. Full site occupancy was fixed for the Sc and O positions and the site occupancy of P/Si was adapted to the stoichiometry.

After refinement of the framework atoms, the occupancy of the atomic positions Na(1) and Na(2) (*6b* and *18e*, respectively) was refined but the obtained Na concentration in the structure model was lower than the Na content determined by ICP-OES. Trying to fix the occupancy at higher values resulted in thermal displacement parameters with negative electron density for at least one of the Na atomic positions. Therefore a third Wyckoff position for Na was introduced in analogy to the structure refinements of $Na_{3.35}Zr_2Si_{2.35}P_{0.65}O_{12}$ [19], corresponding to a displacement of the Na(2) position due to the high mobility of the Na ions in the materials at room temperature. The R_p value then decreased from 12–10% to 7–5% depending on the composition. No other possible Na position could be found.

The ratio of the occupancy of the Na(1), Na(2) and Na(3) positions was fixed as a starting value [19] and adapted to the stoichiometry

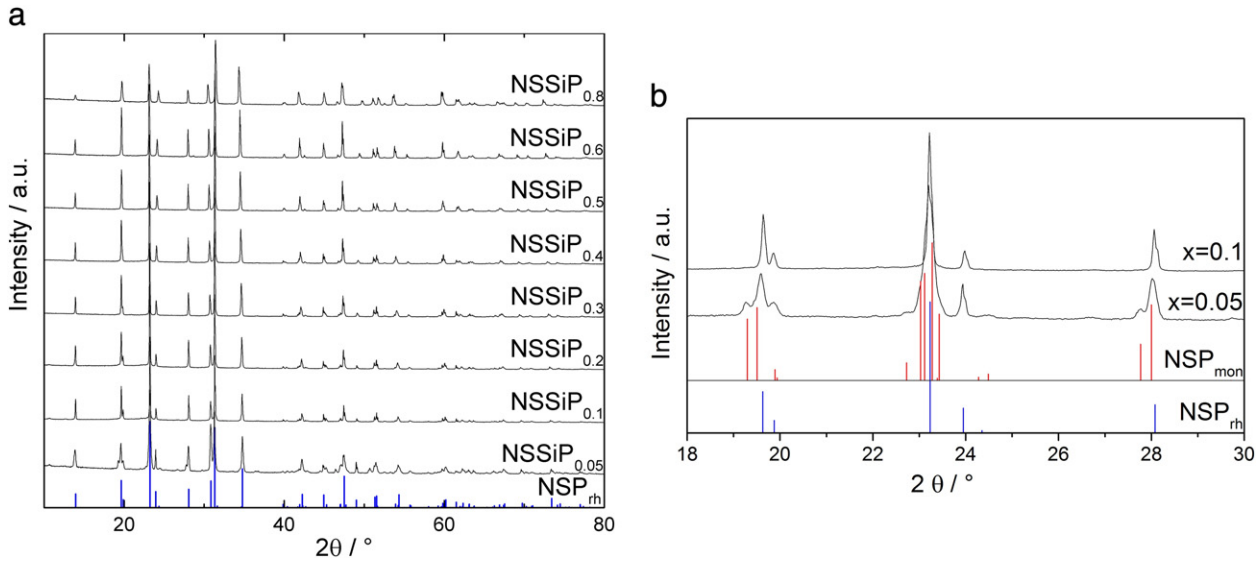

Fig. 1. (a) XRD patterns of $NSSiP_x$ for $0.05 \le x \le 0.8$. (b) Detail of the XRD patterns of $NSSiP_{0.05}$ and $NSSiP_{0.1}$ between $2\theta = 18°$ and 30° and comparison with the XRD patterns of rhombohedral (NSP_{rh}) and monoclinic (NSP_{mon}) $Na_3Sc_2(PO_4)_3$ [17].

determined by ICP-OES. The thermal parameters were refined with fixed occupancy and showed negative values for at least one of the Na positions. The occupancy and the thermal parameters were then alternatively constrained until positive values for all the parameters were obtained. All atomic positions and thermal displacement parameters were then refined with fixed occupancy and the R_p value decreased from approximately 7–5% to 5–4%. The results of the refinement are summarized in Tables 2 and 3.

With increasing Si content, the hexagonal lattice parameters *a* and *c* decrease and increase, respectively. Accordingly, the cell volume increases with the substitution and a plateau is reached at around x = 0.6, as presented in Fig. 2.

The volumes of the ScO_6 octahedra and of the $(P,Si)O_4$ tetrahedra were calculated using the refined data from Tables 2 and 3 and the trend is shown in Fig. 3. An increase in the volume of $(P,Si)O_4$ tetrahedra was observed with the substitution of P with Si. This result agrees with the ionic radii of P and Si in fourfold coordination, i.e. 0.17 Å and 0.26 Å, respectively [8]. In parallel, the volume of the ScO_6 octahedra decreased with the substitution.

3.2. Conductivity measurements

The conductivity measurements were carried out on samples with similar density of 92 to 95%. Fig. 4 shows the dependence of the conductivity at room temperature on the density of the measured pellets of $NSSiP_{0.4}$.

For density values lower than 88% of the theoretical density, the conductivity of the samples is 5 to 8 times lower than for samples with density values between 90 and 96%. Some samples had a density of more than 97% but their conductivity was also 3 to 4 times lower than for those having a density between 90 and 96%. This is probably due to the high anisotropy of the material and the appearance of micro-cracks for highly densified samples having experienced large grain growth [20,21]. As an example, Fig. 5 shows a scanning electron microscopy picture of a fractured pellet of highly densified $NSSiP_{0.4}$. The size of the observed grain is approximately 100 μm whereas the powder before sintering had a mean particle size of 6 μm. The grain growth was considerable for this sample and the resulting micro-cracks in the middle of the large grain are clearly visible. They result from the anisotropic thermal expansion which leads to large residual stresses during cooling (without thermal shock).

A scattering in conductivity data between 4×10^{-4} to 8×10^{-4} S cm^{-1} is observed for samples with densities between 92 to 95% without clear trend. The varying conductivities are also related to the already mentioned cracks as it is difficult to prevent their appearance even with slow cooling rates after the sintering of the samples and with a controlled grain growth.

The impedance spectra show a broad arc that does not meet the origin at high frequency values and a spike at lower frequencies from room temperature to 120 °C. For temperatures above 120 °C, only a straight line was observed. As an example, Fig. 6 represents the impedance spectra of a $NSSiP_{0.4}$ sample at 30 and 300 °C. The fitted parameters are listed in Table 4.

Depending on the temperature, at least two components can be distinguished from the impedance spectra: the bulk resistance at the high frequency intercept and the grain boundary resistance in the broad arc. In the case of $NSSiP_{0.4}$ shown in Fig. 6, the impedance spectrum is fitted with 3 components, the bulk resistance, the grain boundary resistance and the interface between the sample and the blocking electrode. All three processes were fitted by a resistance *R* in parallel with a constant phase element *CPE*. The impedance of the *CPE* is calculated according to:

$$Z_{CPE} = \frac{1}{C_{CPE}(j\omega)^n} \quad (1)$$

where ω is the frequency, *n* is an exponent usually between 1 (corresponding to a pure capacitance) and 0.5 [22] and C_{CPE} is related to the capacitance *C* according to:

$$C = R^{\frac{1-n}{n}} \times C_{CPE}{}^{\frac{1}{n}} [23] \quad (2)$$

When $n \to 1$, then $C_{CPE} \to C$ and an ideal capacitor is observed. A diminishing *n* displays a non-ideal system and $n = 0.5$ corresponds to a pure diffusion process.

The values of capacitance help differentiating the processes observed in the impedance spectra. As a matter of fact, a capacitance around 10^{-12} F is associated with bulk resistance, a value around 10^{-11}–10^{-7} F is associated to the grain boundary resistance and a high capacitance of 10^{-7}–10^{-4} F corresponds to the interface between the sample and the electrode [24].

At high temperature the components corresponding to the bulk resistance and the grain boundary resistance merge. Therefore, only the total resistance, R_{Total}, as a sum of bulk and grain boundary phenomena was deduced from the impedance plot. The low frequency element corresponding to the interface between the sample and the electrode presents a high resistance corresponding to the blocking of mobile ions at the electrode. This value of resistance does not represent the motion of the Na-ions in the sample and is therefore not taken into account in the calculation of the total conductivity.

Table 2
Crystallographic and structural data of the $NSSiP_x$ compounds (standard deviations are given in brackets).

	Compound						
	$NSSiP_{0.1}$	$NSSiP_{0.2}$	$NSSiP_{0.3}$	$NSSiP_{0.4}$	$NSSiP_{0.5}$	$NSSiP_{0.6}$	$NSSiP_{0.8}$
Formula weight [g mol^{-1}]	438.1	441.3	441.2	443.2	448.9	449.7	450.9
Crystal system	Rhombohedral						
Space group, *Z*	R $\bar{3}$c, 6						
a [Å]	8.93926 (3)	8.95795 (4)	8.96890 (4)	8.98000 (2)	8.99614 (4)	9.00460 (3)	9.03343 (2)
c [Å]	22.2735 (1)	22.2601 (2)	22.2388 (2)	22.2212 (1)	22.1528 (2)	22.1261 (1)	21.9901 (1)
V [Å^3]	1541.42 (1)	1546.96 (1)	1549.29 (1)	1551.85 (1)	1552.65 (1)	1553.69 (1)	1554.05 (1)
d_c [g cm^{-3}]	2.8317	2.8422	2.8373	2.8454	2.8806	2.8838	2.8908
Temperature of data collection [K]	298.5						
2θ range [°]	10.00–139.99						
Absorption coefficient, μ [mm^{-1}]	17.718						
Refinement method	Full matrix least square against F^2						
Data points/number of parameters	13,000/23	13,000/23	13,000/23	13,000/23	13,000/23	13,000/23	13,000/23
R_p/R_{wp}/GOF (all data)[a]	6.82/9.24/4.67	5.84/8.54/4.28	5.33/7.76/3.05	4.74/6.39/3.23	5.14/7.15/2.81	4.23/6.01/3.11	4.94/6.72/3.39

[a] $R_p = \Sigma |y_o - y_c| / \Sigma y_o$, $R_{wp} = \Sigma [w(y_o - y_c)^2 / \Sigma w y_o^2]^{1/2}$, $GOF = (R_{wp} / R_{exp})^2$ with $R_{exp} = [(N - P)/\Sigma w y_o^2]^{1/2}$, $w = 1/\sigma^2$.

Table 3
Positional and isotropic displacement parameters [10^4 pm^2] of $NSSiP_x$ with $0.1 \le x \le 0.8$ (standard deviations are given in brackets).

Atom	Wyckoff position	Occupancy	x	y	z	U_{iso}
$NSSiP_{0.1}$						
Sc	*12c*	1	0	0	0.14909(5)	0.0098(2)
P/Si	*18e*	0.9667/0.0333	0.2936(2)	0	0.25	0.0097(4)
O1	*36f*	1	0.1858(3)	−0.0247(3)	0.19403(9)	0.0261(8)
O2	*36f*	1	0.1920(2)	0.1697(2)	0.08660(9)	0.0221(6)
Na1	*6b*	0.4	0	0	0	0.036(3)
Na2	*18e*	0.6167	0.6359(4)	0	0.25	0.029(1)
Na3	*36f*	0.1	0.974(2)	0.726(2)	0.9579(5)	0.019(4)
$NSSiP_{0.2}$						
Sc	*12c*	1	0	0	0.14894(5)	0.00094(2)
P/Si	*18e*	0.9333/0.0667	0.2954(2)	0	0.25	0.0177(4)
O1	*36f*	1	0.1827(3)	−0.0265(3)	0.19410(9)	0.0310(8)
O2	*36f*	1	0.1920(2)	0.1749(2)	0.08672(9)	0.0174(6)
Na1	*6b*	0.47	0	0	0	0.019(2)
Na2	*18e*	0.58	0.6369(5)	0	0.25	0.018(1)
Na3	*36f*	0.13	0.972(1)	0.713(1)	0.9435(4)	0.007(2)
$NSSiP_{0.3}$						
Sc	*12c*	1	0	0	0.14882(5)	0.0127(3)
P/Si	*18e*	0.9/0.1	0.2951(2)	0	0.25	0.0211(4)
O1	*36f*	1	0.1825(3)	−0.0262(3)	0.19383(9)	0.0275(8)
O2	*36f*	1	0.1914(2)	0.1753(2)	0.0865(1)	0.0227(6)
Na1	*6b*	0.51	0	0	0	0.021(2)
Na2	*18e*	0.5267	0.6394(5)	0	0.25	0.014(1)
Na3	*36f*	0.155	0.972(1)	0.703(1)	0.9409(4)	0.006(2)
$NSSiP_{0.4}$						
Sc	*12c*	1	0	0	0.14889(3)	0.0099(2)
P/Si	*18e*	0.8667/0.1333	0.2956(1)	0	0.25	0.0161(2)
O1	*36f*	1	0.1846(2)	−0.0252(2)	0.19441(6)	0.0272(5)
O2	*36f*	1	0.1905(2)	0.1728(2)	0.08634(6)	0.0158(4)
Na1	*6b*	0.52	0	0	0	0.022(1)
Na2	*18e*	0.5567	0.6389(3)	0	0.25	0.0138(7)
Na3	*36f*	0.155	0.9724(9)	0.7076(8)	0.9431(2)	0.016(2)
$NSSiP_{0.5}$						
Sc	*12c*	1	0	0	0.14834(5)	0.0109(2)
P/Si	*18e*	0.8333/0.1667	0.2953(1)	0	0.25	0.0166(3)
O1	*36f*	1	0.1847(3)	−0.0227(3)	0.19347(9)	0.0251(7)
O2	*36f*	1	0.1919(2)	0.1716(2)	0.0873(1)	0.0180(5)
Na1	*6b*	0.64	0	0	0	0.021(2)
Na2	*18e*	0.61	0.6416(5)	0	0.25	0.016(1)
Na3	*36f*	0.145	0.982(1)	0.705(1)	0.9407(4)	0.007(2)
$NSSiP_{0.6}$						
Sc	*12c*	1	0	0	0.14831(4)	0.0108(2)
P/Si	*18e*	0.8/0.2	0.2942(1)	0	0.25	0.0165(3)
O1	*36f*	1	0.1898(2)	−0.0201(2)	0.19320(8)	0.0221(6)
O2	*36f*	1	0.1900(2)	0.1712(2)	0.08645(9)	0.0192(4)
Na1	*6b*	0.7	0	0	0	0.026(1)
Na2	*18e*	0.62	0.6423(3)	0	0.25	0.0110(8)
Na3	*36f*	0.14	0.983(1)	0.697(1)	0.9449(3)	0.01(2)
$NSSiP_{0.8}$						
Sc	*12c*	1	0	0	0.14823(3)	0.0098(2)
P/Si	*18e*	0.7333/0.2667	0.2978(1)	0	0.25	0.0129(2)
O1	*36f*	1	0.1872(2)	−0.0192(3)	0.19312(7)	0.0287(6)
O2	*36f*	1	0.1889(2)	0.1710(2)	0.08536(7)	0.0109(4)
Na1	*6b*	0.72	0	0	0	0.0090(8)
Na2	*18e*	0.67	0.6422(4)	0	0.25	0.0202(9)
Na3	*36f*	0.13	0.947(1)	0.699(1)	0.9351(4)	0.016(3)

The conductivity was then calculated according to the expression:

$$\sigma_{Total} = \frac{l}{A \times R_{Total}} \quad (3)$$

where l is the thickness of the measured pellet and A the area of the electrode.

The Arrhenius plot of the total conductivity of the $NSSiP_x$ materials for $0.1 \le x \le 0.8$ is shown in Fig. 7.

A change in slope was observed for all compositions at around 200 °C, but no phase transition was detected by TG/DSC or high-temperature XRD measurements. The change in slope is explained by the diminishing contribution of the grain boundary conductivity with increasing temperature as described for β-alumina by Hooper [25], where the activation energies of single crystals and polycrystalline samples were compared and matched at high temperature.

To verify this hypothesis, more data where gathered by measuring the conductivity of the materials from −30 °C to 30 °C. From −30 °C

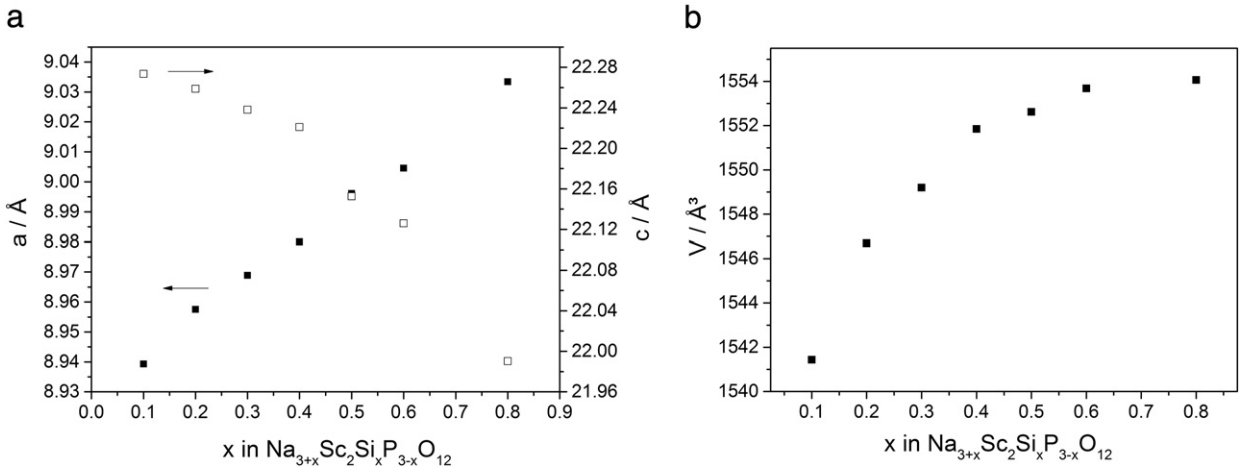

Fig. 2. (a) Lattice parameters and (b) cell volume as a function of x in $NSSiP_x$.

to 0 °C, 2 semi-circles are observed and can be attributed to the bulk resistance and the grain boundary resistance as shown in Fig. 8. The corresponding fitted impedance parameters are listed in Table 5.

The values of capacitance seem to validate the interpretation of bulk and grain boundary resistance in the impedance spectra [24] and in the following $R_1 = R_{bulk}$ and $R_2 = R_{GB}$. The values of conductivity for the bulk and the grain boundary conduction are both normalized to the sample dimensions according to Eq. (3). The value of $\sigma_{Grain\ boundary}$ in the following is therefore not the local grain boundary conductivity but an effective average value of all grain boundaries in the sample.

The ratio R_{bulk}/R_{GB} increases with increasing temperature (0.06 for −30 °C, 0.1 for −20 °C and 0.16 for −10 °C in the case of $NSSiP_{0.4}$), indicating that at low temperatures the contribution of the grain boundary resistance to the overall resistance first increases due to the lower conductivity but higher activation energy and then diminishes with further increase of temperature due to the decreasing contribution to the overall resistance. This also explains the change of slope in the Arrhenius plot seen in Fig. 7. The evolution of the capacitance and the exponent *n* with the temperature (Table 5) is not clear within 20 °C of temperature differences but it is expected that *n* diminishes with increasing temperature since the system becomes less and less ideal. This is observed at 30 °C in Fig. 6 where $n_1 = n_{bulk} = 0.53$ and no complete semi-circle is observed.

Fig. 9 represents the Arrhenius plot for the bulk conductivity and the grain boundary conductivity.

The experimental data were fitted to the Arrhenius expression

$$\sigma T = Ae^{\frac{-Ea}{kT}} \quad (4)$$

to determine the activation energy. Here, σ is the conductivity of the sample, *A* is the pre-exponential factor, *k* is the Boltzmann constant, and *T* is the absolute temperature. Fig. 10(a) represents the evolution of the total conductivity at 30 °C and at 300 °C vs. the amount of Si per formula unit, as well as the evolution of the activation energy of total conductivity up to 200 °C. The conductivity and activation energy values of the end member of the solid solution, $Na_3Sc_2(PO_4)_3$, were taken from Winaud et al. [11]. The evolution of the bulk conductivity at 25 °C extrapolated from Eq. (4) and of the activation energy of the bulk conductivity as well as the activation energy of the total conductivity from 200 °C to 400 °C are shown in Fig. 10(b).

The total conductivity increases with the substitution of P with Si and the conductivity values for $0.1 \le x \le 0.5$ are in the same range. For $x > 0.5$, the conductivity drops in correlation with the decreasing amount of Na vacancies as well as the structural parameters as described hereafter. The bulk conductivity follows the same trend but a steeper increase and decrease of conductivity is observed around the maximum conductivity at $0.3 < x < 0.4$.

The activation energy decreases with increasing x up to $x = 0.3$, after which the values lie in the same range for the low-temperature data of

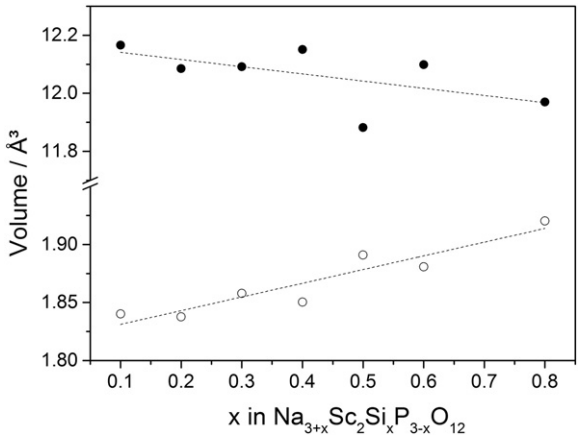

Fig. 3. Evolution of the volume of the ScO_6 octahedra (filled symbols) and $(P,Si)O_4$ tetrahedra (open symbols) with increasing Si content.

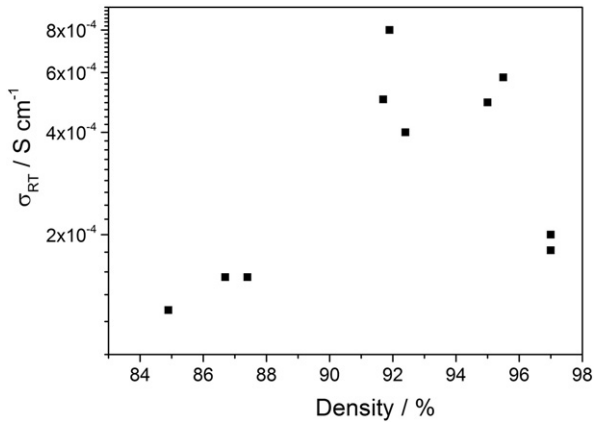

Fig. 4. Influence of the density of pellet samples on the total conductivity.

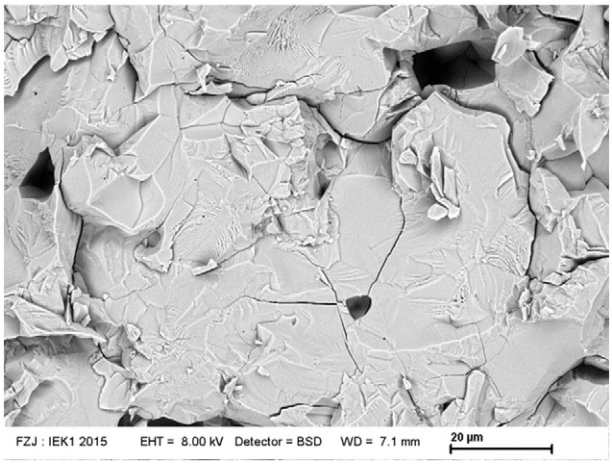

Fig. 5. SEM picture of a crack inside a grain of a highly sintered $NSSiP_{0.4}$ sample.

the total conductivity. The determined values of 0.3–0.35 eV have been reported very often for highly conductive NASICON materials [7].

The activation energy of the bulk conductivity, however, is significantly smaller and correlates better with the conductivity values since an increase was observed for $x > 0.5$. In addition, the values correspond to similarly low values observed for the lithium-analogue $Li_{1+x}Al_xTi_{2-x}P_3O_{12}$ [26,27]. The impact of the grain boundary conductivity varies for each composition and influences the total conductivity (and accordingly the activation energy) which explains the better correlation of the bulk data. Finally, the activation energy at high temperature follows roughly the same trend as the activation energy of the bulk conductivity and also increases for $x > 0.5$ and only the end members of the series have matching activation energies as outlined by Hooper [23]. The activation energies at high temperature are lower than the data of the total conductivity at low temperature and higher than the data from bulk conductivity. This indicates that between 200 °C and 400 °C the contribution of the grain boundary conductivity is decreasing but not completely negligible. It can be expected that the activation energy of the bulk conductivity and of the total conductivity match at even higher temperatures.

Table 4
Fitted data of impedance spectra of $NSSiP_{0.4}$ shown in Fig. 6. The capacitance values are calculated according to Eq. (2).

T/°C	R/Ω	$C_{CPE}/\Omega^{-1}\,s^n$	Exponent n	C/F
300	$R_1 = 13$			
	$R_2 = 1.2 \times 10^{12}$	$C_{CPE1} = 4.0 \times 10^{-5}$	$n_1 = 0.88$	4.2×10^{-4}
30	$R_1 = 254$	$C_{CPE1} = 2.0 \times 10^{-7}$	$n_1 = 0.53$	3.1×10^{-11}
	$R_2 = 289$	$C_{CPE2} = 6.7 \times 10^{-7}$	$n_2 = 0.85$	1.5×10^{-7}
	$R_3 = 1.6 \times 10^{12}$	$C_{CPE3} = 2.1 \times 10^{-5}$	$n_3 = 0.85$	4.5×10^{-4}

The highest total conductivity of 6.9×10^{-4} S cm^{-1} for $x = 0.4$ at 25 °C places $NSSiP_{0.4}$ among the ten best NASICON sodium-conductive materials reported to date [7].

3.3. Correlation between composition, crystal structure and conductivity

Substituting Si in $Na_3Sc_2(PO_4)_3$ has two simultaneous impacts: a) the change in the Na content and hence the increase in charge carriers and b) the change in lattice size and hence the steric (but also electrostatic) change along the conduction paths. Both impacts influence the conductivity of the compounds.

3.3.1. Na content

Increasing the amount of charge carriers increases the conductivity of the material as it was observed for compositions up to 3.4 mol Na per formula unit in the nominal stoichiometry. For higher Na concentrations, the conductivity decreases due to the decreasing amount of Na vacancies. A balance between the amount of occupied and vacant Na sites is crucial for a high ionic conductivity. In $NSSiP_x$, the maximal amount of Na per formula unit is 4 mol and the highest conductivity is achieved around 3.12 mol (ICP-OES data see Table 1) which represents a ratio of occupied Na sites over vacant Na sites of approximately 80/20: the conductivity increases with the amount of charge carriers but at least 20% of the charge carrier positions have to be vacant. This result agrees with the trend observed by Vogel et al. [12] since the highest conductivities and lowest activation energies were obtained for an amount of 3.2–3.5 mol Na per formula unit in the series $Na_{1+x}Hf_2Si_xP_{3-x}O_{12}$.

For more precise refinement of the sodium occupancy, neutron diffraction data would be more suitable, but using the Rietveld refinements as a first approximation, the most conductive compound – in this study $NSSiP_{0.4}$ – has 50 and 85% occupancy of the Na(1) and

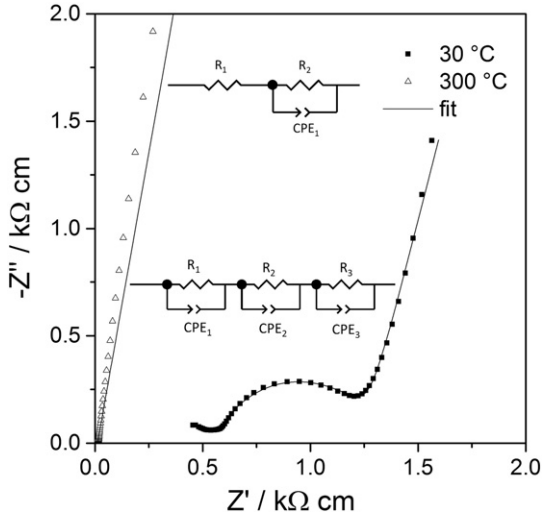

Fig. 6. Impedance spectra of a $NSSiP_{0.4}$ sample at 30 and 300 °C. The fitted parameters of the equivalent circuits shown here are listed in Table 4.

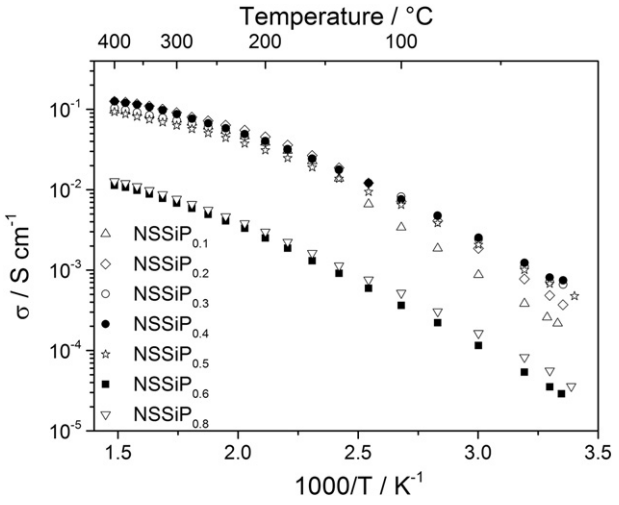

Fig. 7. Arrhenius plot of the conductivity of $NSSiP_x$ with $0.1 \le x \le 0.8$ from 30 °C to 400 °C.

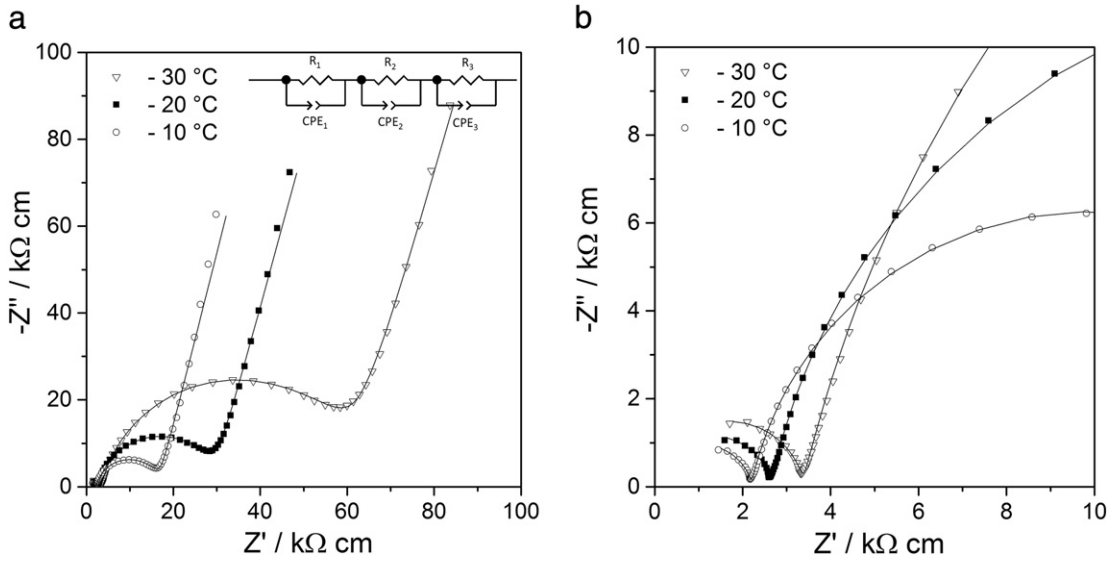

Fig. 8. Impedance spectra of a $NSSiP_{0.4}$ sample at −30, −20 and −10 °C for (a) the whole frequency range and (b) the high frequency part. The fitted parameters of the equivalent circuit shown in (a) are listed in Table 5.

Na(2) + Na(3) Wyckoff positions, respectively. This means that $(0.5 + 3 \times 0.85)/4 \times 100 = 76\%$ of the sites are occupied.

3.3.2. Lattice size

The change in lattice size directly influences the size of the pathway for the Na^+ conduction and the hopping distance of the Na^+ ions to the next vacancy.

3.3.3. Distance Na(1)–Na(2)

The Na^+ conduction occurs by successive hopping from the Na(1) to the Na(2) Wyckoff positions. Therefore, the impact of the distance between these positions determined at room temperature on the activation energy of the bulk conductivity measured between −30 and 0 °C was investigated. The small deviations of the distances due to the influence of thermal expansion do not change the general feature of Fig. 11.

An increasing hopping distance for the Na^+ ions is not favorable and leads to a high activation energy. In the case of $NSSiP_x$, the activation energy for the Na conduction rises when the distance between the positions Na(1) and Na(2) exceeds 3.433 Å. For smaller Na(1)–Na(2) the activation energies slightly increase with shorter distances. Therefore only a tentative optimal distance at about 3.42–3.43 Å leading to the lowest activation energy can be deduced from Fig. 11. The same correlation was observed between the Na(1) and the Na(3) position since the position Na(3) is only a displacement of the Na(2) position.

Table 5
Fitted data of impedance spectra of $NSSiP_{0.4}$ shown in Fig. 8. The capacitance values are calculated according to Eq. (2).

T/°C	R/Ω	$C_{CPE}/\Omega^{-1}\,s^n$	Exponent n	C/F
−30 °C	$R_1 = 799$	$C_{CPE1} = 2 \times 10^{-10}$	$n_1 = 0.92$	1.2×10^{-11}
	$R_2 = 13{,}528$	$C_{CPE2} = 3 \times 10^{-7}$	$n_2 = 0.86$	2.8×10^{-8}
	$R_3 = 7.7 \times 10^{12}$	$C_{CPE3} = 1 \times 10^{-5}$	$n_3 = 0.83$	9.7×10^{-5}
−20 °C	$R_1 = 627$	$C_{CPE1} = 3 \times 10^{-10}$	$n_1 = 0.91$	1.5×10^{-11}
	$R_2 = 6270$	$C_{CPE2} = 3 \times 10^{-7}$	$n_2 = 0.88$	3.0×10^{-8}
	$R_3 = 3.9 \times 10^{13}$	$C_{CPE3} = 1 \times 10^{-5}$	$n_3 = 0.83$	1.3×10^{-4}
−10 °C	$R_1 = 522$	$C_{CPE1} = 3 \times 10^{-10}$	$n_1 = 0.90$	1.3×10^{-11}
	$R_2 = 3407$	$C_{CPE2} = 3 \times 10^{-7}$	$n_2 = 0.88$	2.9×10^{-8}
	$R_3 = 2.1 \times 10^{13}$	$C_{CPE3} = 1 \times 10^{-5}$	$n_3 = 0.84$	9.0×10^{-5}

3.3.4. Bottleneck of Na conduction

The pathway of Na^+ ions in the structure has already been described in the first NASICON material by Hong et al. [1,2]. The Na^+ ions have to pass through two triangles of oxygen from the 6*b* to the 18*e* site. Later, Losilla et al. [28] tried to correlate the activation energy with the area of the smallest triangle, T1, for $Na_{1.4}In_{0.4}M_{1.6}(PO_4)_3$ (M = Ti, Sn, Hf, Zr). This correlation was validated for approximately 30 NASICON materials with reported structural parameters [7].

Using the refined crystal structure of the $NSSiP_x$ compounds, the area of the T1 triangle was calculated and correlated with the values of activation energy of the total conductivity determined at low temperature. This correlation was then compared with the data of Losilla et al. [28] as well as those of the solid solution of scandium-substituted NASICONs, $Na_{1+x+y}Zr_{2-x}Sc_x(SiO_4)_y(PO_4)_{3-y}$ [1,14], since in these reports only the activation energy of the total conductivity was used. The results are presented in Fig. 12 and a fairly good linear correlation is obtained ($R^2 = 0.87$).

The trend is similar to other NASICON materials: the activation energy decreases when the T1 area increases. However, taking a closer look only at the $NSSiP_x$ materials, the correlation is no longer clear. On the one hand, it should be kept in mind that for all datasets shown in Fig. 12, the activation energies are spoiled with the varying grain boundary contributions for each composition. On the other hand, the activation energy values are in the same range as well as the T1 areas so that the experimental error in determining the activation energy and structural parameters do not result in a clear correlation. In the refined data of $NSSiP_x$ the standard deviation of the position of the oxygen atoms added to the ones of the lattice parameters gave an error on the area T1 of approximately 0.065 $Å^2$. As an example, the error bar for the sample $NSSiP_{0.2}$ is depicted in Fig. 12. A better correlation can be expected for using only the activation energy of the bulk conductivity but the scattering of data will still be large due to the errors of the area T1 and of the activation energy for the bulk conductivity.

To assess whether other geometrical parameters could also block the conduction pathway of the Na^+ ions, the impact of the interatomic distance between the Na ions and the next oxygen atoms was studied, as depicted in Fig. 13.

The distance between the Wyckoff position Na(1) and the top of the T2 triangle O(2) was investigated as well as the distance between the Wyckoff position Na(2) and the top of the T1 triangle O(1). The results are plotted in Fig. 14.

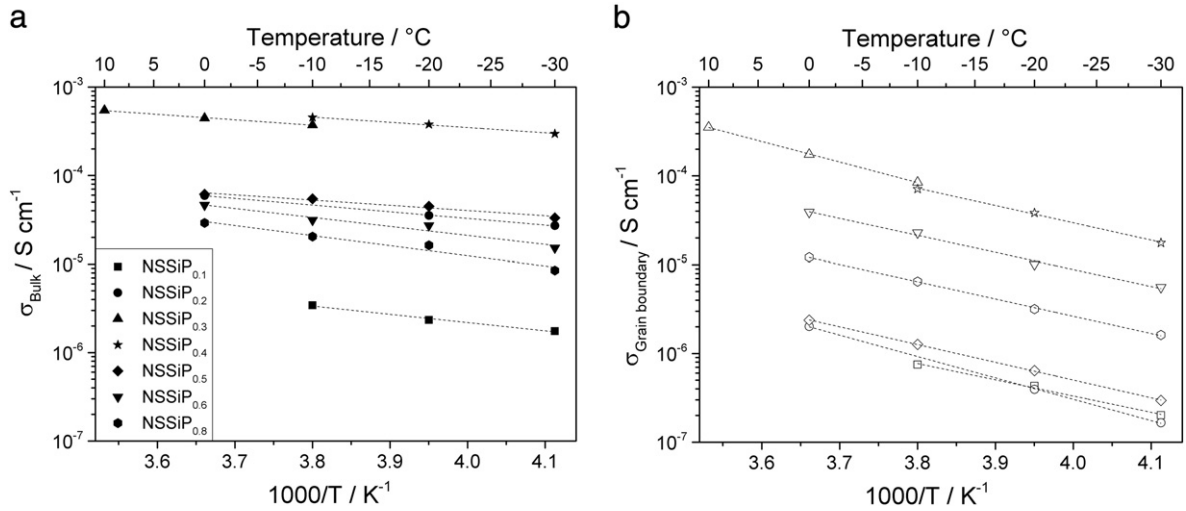

Fig. 9. Arrhenius plot for (a) the bulk conductivity of the NSSiP$_x$ samples and (b) the grain boundary conductivity.

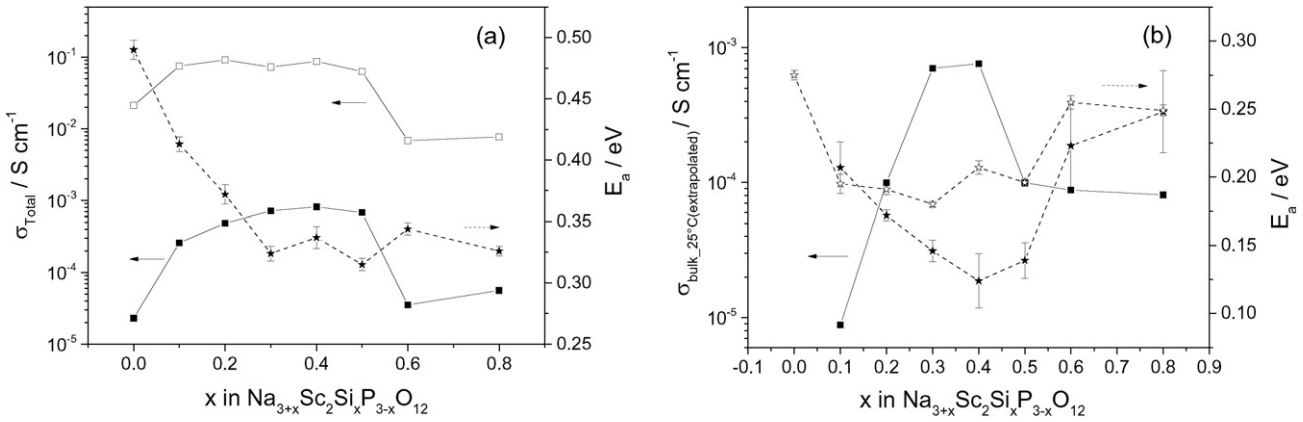

Fig. 10. Dependence of conductivity and activation energy with the amount of Si content in the NSSiP$_x$ materials: (a) total conductivity at 30 °C (filled squares), total conductivity at 300 °C (open squares) and the activation energy at low temperature (filled stars); (b) extrapolated bulk conductivity at 25 °C (filled squares) and the activation energy of the bulk conductivity (filled stars) as well as the activation energy of the total conductivity at high temperature (200–400 °C; open stars).

The correlation between the activation energy and the Na—O distances seems to reflect a reasonable linearity, even if a significant scatter was observed. Fig. 14 also shows that both Na—O distances show the same slope although the distances of the two datasets differ by about 0.2 Å. In the case of NSSiP$_x$, it appears that the bottleneck is merely determined by the T1 area, but rather by the Na^+–O^{2-} distances and the mobility is enhanced when the distances are large.

4. Conclusion

Substituting P with Si in the ion-conductive $Na_3Sc_2(PO_4)_3$ [11] leads to $Na_{3.4}Sc_2(SiO_4)_{0.4}(PO_4)_{2.6}$ with very high sodium ion conductivity of $\sigma_{Na,Total} = 6.9 \times 10^{-4}$ S cm^{-1} at 25 °C. The systematic study of the solid solution $Na_{3+x}Sc_2(SiO_4)_x(PO_4)_{3-x}$ with $0.05 \le x \le 0.8$ led to a better understanding of the influence of the substitution of P with Si in the NASICON materials. The increase in charge carriers led to an increase in conductivity until a maximum was reached, after which the ratio of the amount of charge carriers to vacancies was not favorable.

Correlations between the activation energy and the lattice parameters for the experimentally produced data revealed the existence of optimal lattice parameters. The change in lattice size directly influenced the size of the pathway for the Na^+ conduction and the hopping distance of the Na^+ ions to the next vacancy. A hopping distance that is too long requires a high activation energy for the conduction, which was observed for the compounds $Na_{3.6}Sc_2(SiO_4)_{0.6}(PO_4)_{2.4}$ and $Na_{3.8}Sc_2(SiO_4)_{0.8}(PO_4)_{2.2}$. Furthermore, the influence of the size of the smallest triangle of oxygen atoms through which the Na^+ ions have to

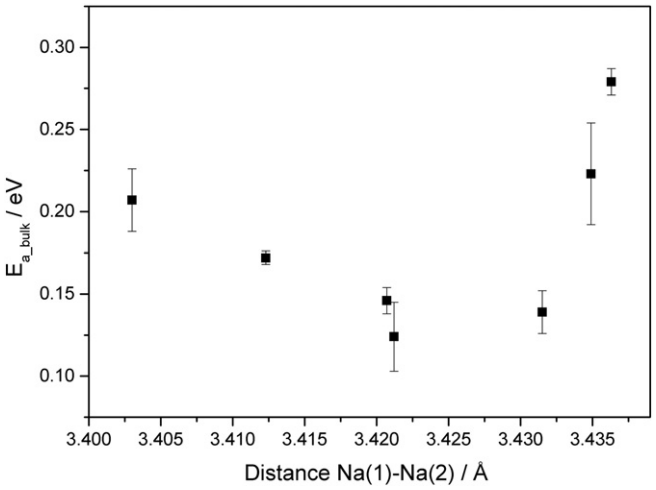

Fig. 11. Correlation between the activation energy and the interatomic distance between the Wyckoff positions Na(1) and Na(2).

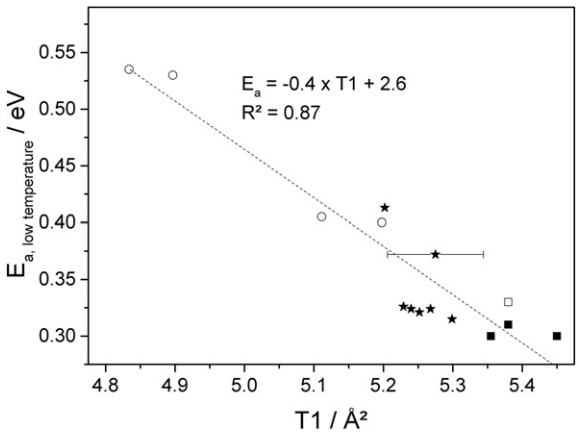

Fig. 12. Activation energy of total conductivity as a function of the T1 area for $NSSiP_x$ (filled stars), $Na_{1+y+z}Zr_{2-y}Sc_y(SiO_4)_z(PO_4)_{3-z}$ [14] (filled squares), $Na_3Zr_2(SiO_4)_2(PO_4)$ [1] (open square) and $Na_{1.4}M_{1.6}In_{0.4}(PO_4)_3$ [27] (open circles).

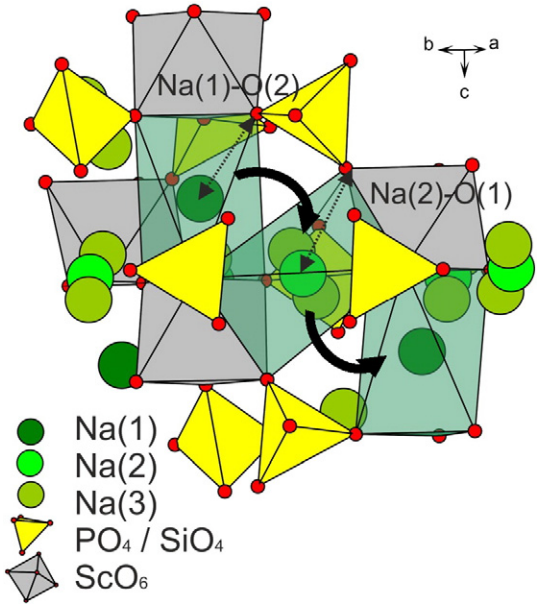

Fig. 13. Representation of the conduction pathway in the NASICON structure along $(5\ 3\ \bar{1})$ using the crystallographic data of $NSSiP_{0.3}$.

jump, assumed as the bottleneck for diffusion, was validated for this solid solution and other NASICON materials found in the literature. The distance between the charge carriers to the nearest oxygen atoms, however, seems to be more important.

For better insights into the discussed correlations, neutron scattering data or XRD measurements on single crystals would allow a higher precision of the atomic positions and particularly the occupancies in

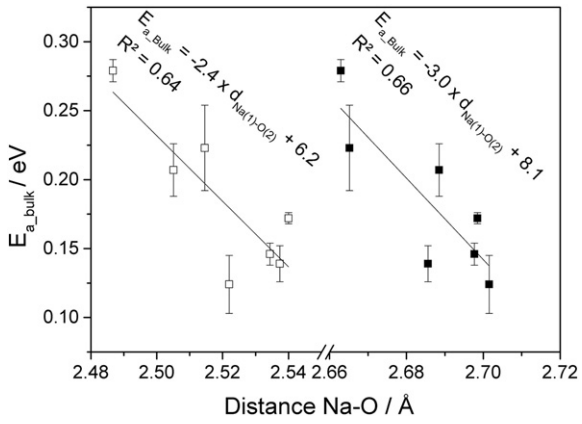

Fig. 14. Correlation between the activation energy and the interatomic distance between the Na atoms and the next oxygen atoms in the structure: the open symbols represent the impact of the distance between Na(1) and O(2) and the filled symbols the distance between Na(2) and O(1).

the NASICON materials. The variation of Na concentration is currently under investigation to better understand the impact of Na excess and deficiency on the ionic conductivity of these materials.

References

[1] H.Y.P. Hong, Mater. Res. Bull. 11 (1976) 173–182.
[2] H.Y.P. Hong, J.B. Goodenough, J.A. Kafalas, Mater. Res. Bull. 11 (1976) 203–220.
[3] F. Lalère, J.B. Leriche, M. Courty, S. Boulineau, V. Viallet, C. Masquelier, V. Seznec, J. Power Sources 247 (2014) 975–980.
[4] H. Zhang, J. Li, H. Zhang, X. Liang, C. Yin, Q. Diao, J. Zheng, G. Lu, Sensors Actuators B Chem. 180 (2013) 66–70.
[5] H.-Y. Dang, X.-M. Guo, Sensors Actuators B Chem. 178 (2013) 163–168.
[6] Y. Shimizu, S. Takase, K. Ida, M. Imamura, I. Koguma, Key Eng. Mater. 412 (2009) 107–111.
[7] M. Guin, F. Tietz, J. Power Sources 273 (2015) 1056–1064.
[8] R.D. Shannon, Acta Crystallogr. A32 (1976) 751–767.
[9] M.S. Whittingham, R.A. Huggins, J. Chem. Phys. 54 (1971) 414–416.
[10] J.L. Briant, G.C. Farrington, J. Solid State Chem. 33 (1980) 385–390.
[11] J.M. Winaud, A. Rulmont, P. Tarte, J. Mater. Sci. 25 (1990) 4008–4013.
[12] E.M. Vogel, R.J. Cava, E. Rietman, Solid State Ionics 14 (1984) 1–6.
[13] L. Boehm, C.J. Delbecq, E. Hutchinson, S. Susman, Solid State Ionics 5 (1981) 311–314.
[14] M.A. Subramanian, P.R. Rudolf, A. Clearfield, J. Solid State Chem. 60 (1985) 172–181.
[15] P.J. Squattrito, P.R. Rudolf, P.G. Hinson, A. Clearfield, K. Volin, J.D. Jorgensen, Solid State Ionics 31 (1988) 31–40.
[16] V. Petricek, M. Dusek, L. Palatinus, Z. Krist. 229 (2014) 345–352.
[17] J.-P. Boilot, P. Colomban, G. Collin, R. Comes, J. Phys. Chem. Solids 47 (1986) 843–854.
[18] R.A. Young, The Rietveld Method, Oxford University Pr., Oxford, 1993.
[19] J.P. Boilot, G. Collin, P. Colomban, J. Solid State Chem. 73 (1988) 160–171.
[20] J.E. Blendell, R.I. Coble, J. Am. Ceram. Soc. 65 (1982) 174–178.
[21] S.D. Jackman, R.A. Cutler, J. Power Sources 218 (2012) 65–72.
[22] A. Lasia, Electrochemical Impedance Spectroscopy and its Applications in Modern Aspects of Electrochemistry, Kluwer Academic/Plenum Publishers, New York, 1999.
[23] P. Hjalmarsson, M. Søgaard, M. Mogensen, Solid State Ionics 180 (2009) 1395–1405.
[24] J.T.S. Irvine, D.C. Sinclair, A.R. West, Adv. Mater. 2 (1990) 132–138.
[25] A. Hooper, J. Phys. D. Appl. Phys. 10 (1977) 1487–1496.
[26] Y. Yoon, J. Kim, C. Park, D. Shin, J. Ceram. Process. Res. 14 (2013) 563–566.
[27] M. Kotobuki, M. Koishi, Ceram. Int. 39 (2012) 4645–4649.
[28] E.R. Losilla, M.A.G. Aranda, S. Bruque, A.R. West, Chem. Mater. 10 (1998) 665–673.